Journal of Physics Communications

PAPER • OPEN ACCESS

The optical properties of the Woodburytype—an alternative printing technique based on a gelatine/pigment matrix

To cite this article: D J Leech *et al* 2020 *J. Phys. Commun.* **4** 015018

View the article online for updates and enhancements.

This content was downloaded from IP address 164.11.186.131 on 30/01/2020 at 15:51

Journal of Physics Communications

OPEN ACCESS

RECEIVED
21 October 2019

REVISED
20 January 2020

ACCEPTED FOR PUBLICATION
22 January 2020

PUBLISHED
29 January 2020

Original content from this work may be used under the terms of the Creative Commons Attribution 4.0 licence.

Any further distribution of this work must maintain attribution to the author(s) and the title of the work, journal citation and DOI.

PAPER

The optical properties of the Woodburytype—an alternative printing technique based on a gelatine/pigment matrix

D J Leech[1], **W Guy** and **S Klein**

Centre for Fine Print Research, University of the West of England, Bristol BS3 2JT, United Kingdom
[1] Author to whom any correspondence should be addressed.

E-mail: Damien.Leech@uwe.ac.uk, Walter2.Guy@uwe.ac.uk and Susanne.Klein@uwe.ac.uk

Keywords: print, Kubelka-Munk, gelatine, Woodburytype, carbon black, relief print

Abstract

The Woodburytype is a 19th century photomechanical printing method, producing high-quality continuous-tone images that use a suspension of carbon black in gelatine as a relief print, in which the variation in height of the print produces the grayscale and contrast. We propose a phenomenological optical model for the process based on Kubelka-Munk theory that considers the ink formulation, the print height and the substrate surface in order to provide the ideal combination of printing depth and contrast.

1. Introduction

Printing methods have traditionally been utilised to mass produce items and images—at a low cost and with a large throughput. Both traditional and modern processes, including screen, gravure and inkjet printing, have been exploited and re-purposed across a broad number of fields, such as the production of flexible electronics [1], biosensors [2] and optical lenses [3]. Therefore, research into alternative print processes can be seen, not only as a route for obtaining a high-quality reproduction of an image, but also as a broader fabrication technique.

In 1864, Walter B. Woodbury patented a method to print continuous tone photographic images from an intaglio/relief printing plate [4–7]. He licensed his method to different companies. When H. Barden Pritchard visited The Woodbury Permanent Printing Company at Kent Gardens in 1882, he reported that 30,000 prints could be pulled in a day, which made them the main supplier for portraits between electioneering orders and orders connected with Royal marriages [8]. Pritchard described the steps for Woodburytype in an industrial setting as follows:

- A light sensitive gelatine film is put under a negative in a printing frame and printed in the Sun.
- The unhardened gelatine is washed off in warm water. After hardening with alum, the film is mounted on a glass plate to dry.
- The dry film is stripped off and transferred into a steel tray.
- The steel tray is put into a press and a lead plate is pushed into the tray with a pressure between 150–500 tons which transfer the gelatine relief onto the lead plate. This is repeated until enough lead plates are produced to fill the Woodbury printing press.
- The commercial Woodbury printing process consisted of a table on a revolving pivot with a number of printing presses mounted at the margin. The printer opens each press, pours warm pigmented gelatine on the oiled lead plate, puts a piece of paper on top, closes the press and rotates the table to repeat the procedure until they reach the first press again, at which point the gelatine ink has solidified enough for the print to be removed. The cycle begins again.

© 2020 The Author(s). Published by IOP Publishing Ltd

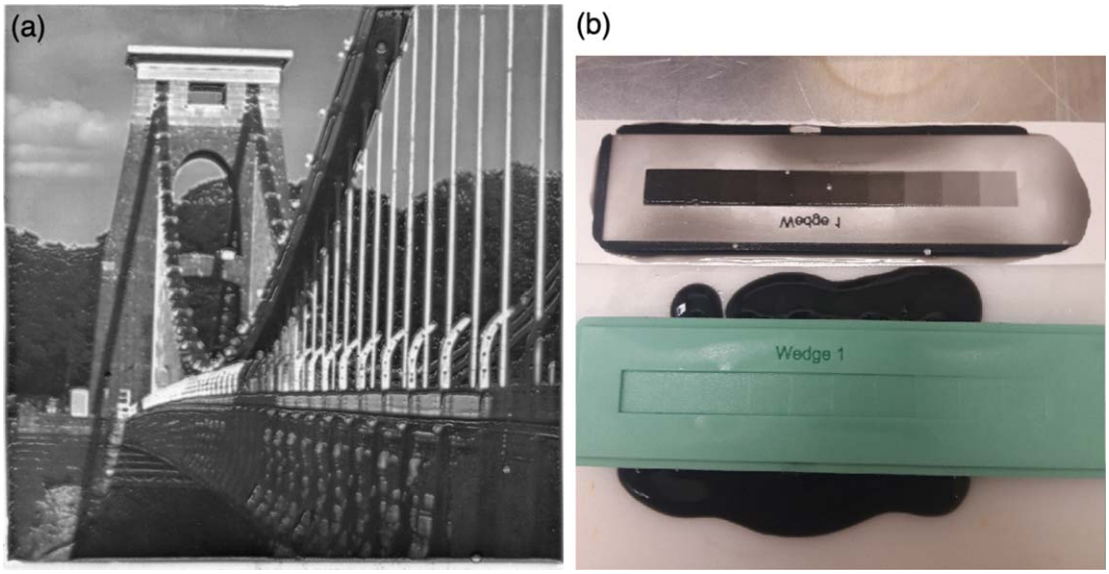

Figure 1. Two examples of the Woodburytype print, using inks with a pigment concentration of 0.015% (a) and 0.025% (b). (a) displays how a high quality photographic image, including fine details such cables on the bridge, can be reproduced using this method. (b) displays the most simple example of how plate depth is directly tied to lightness of the print in this process, whereby a plate with ten steps, ranging from 0.1 to 1 mm in depth, translates into an image. The deepest steps (∼1 mm) produce the darkest steps on the image, whilst the shallowest steps (∼0.1 mm) produce the lightest steps on the image.

- After the print is removed, it is transferred to another room where it is dried, hardened, trimmed and mounted.

Commercial Woodburytype printing had disappeared by around 1900 [9]. The labour intensive post-processing of the print (the hardening, trimming and mounting) made it too costly to compete with half-toning prints [10], where no post-processing was required and text and images could be printed at the same time. A comprehensive discussion of the history and the process itself can be found in [6] and an example of the quality and detail achievable within the process can be seen in figure 1(a).

This process utilises the quick-setting nature of gelatine films, that mean they begin to flow at reasonable temperatures ($T \approx$ 40–60 °C), gel quickly and provide colloidal stability. These features of gelatine films have been more traditionally utilised in photography [11] and food science [12], but recent interest in the material stems mostly from the biosciences, such as biomimetics [13], biomedical purposes [14] and biosensors [15]. The thin, finely patterned films of gelatine produced by the Woodburytype process may be of use to practitioners of these fields that require more bespoke and detailed structural and optical properties of the films.

Modern Woodburytype practices no longer require the lead plate, instead the most common modern practice to manufacture a Woodbury printing plate is to use a CNC mill to engrave the image directly onto the printing plate [7, 16]. The print is pulled from this milled printing plate or a silicon cast of the plate, which are filled with a pigmented gelatine ink.

The tonal qualities of the print are achieved by variations of the print height and therefore of the probability that photons are absorbed or scattered as they pass through the print. The higher the attenuation coefficient and the longer the light path through the medium, the darker the tone. We suggest a simple and empirical optical model to predict the optimal carbon black pigment concentration for a given printing plate depth in order to achieve the largest possible contrast and grayscale—which is currently the most involved and time-consuming process in the printing cycle. This is primarily due to the non-linear interplay between the plate depth and the apparent lightness of the print produced which, in combination with the small amounts of pigment used, mean that small variations in either variable can lead to vastly different lightness values. In addition to this, an ink formulation is only optimal for printing plates with the same range of depths embedded in the plate, therefore a new plate with a new minimum and maximum depth will require a new ink formulation.

2. Experimental methods—ink formulation & optical measurements

2.1. Ink formulation

Historic ink formulations, seen in [17], and x-ray fluorescence analysis and attenuated total reflectance Fourier-transform infrared spectroscopy, as in [18], show that Woodburytype inks in prints historically contain gelatine

and pigment—lacking the more typical imaging metals, such as in silver halide photographic prints. Despite the vast history that gelatine has as a photosensitive material [19], we use it here only as a binder for the ink, as upon heating above ~40°C it flows easily and can be stored as a 'frozen' solution in the fridge (~6 °C), where it sets to a gel. Additionally, it is fairly uniformly transparent in the visible region [20] and so provides less optical interaction with the pigment used.

The gelatine inks for Woodburytype used in our formulation consist of roughly 17.5 wt% of gelatine and 82.5 wt% of de-ionised water, pigmented with the addition of 0.005 to 0.1 wt% of carbon black. Pigment concentrations outside these bounds result in prints that are obviously visually defective, either being too light or too dark, with a minimal grayscale gamut. Additionally, this ratio of gelatine to water allows for prints that set at room temperature within minutes and inks that flow well at ~40 °C. A constant ratio (and therefore concentration) of the gelatine and the water is maintained in order to ensure structural properties [21] and, more importantly, the print heights are kept constant. The gelatine used was Rousselot 250 LB 8 gelatine with a bloom of 250 (made from bovine bones, used as received) and the carbon black was XPB 430 (Orion engineered carbon, used as received), an easy to disperse carbon black pigment preparation with 50 wt% pigment content.

Half of the de-ionised water is added to the gelatine and the mixture left to swell. The pigment is dispersed in the rest of the water and added to the water gelatine mixture, when all previously added water has been absorbed by the gelatine. The final mixture is melted in a low temperature oven at 50 °C. After printing, several hours are required for the print to reach the equilibrium point for water evaporation for a standard sized print in ambient conditions—in practice the print is left to dry overnight.

2.2. Printing process

In order to obtain quantitative data, we use a step-wedge silicon printing plate that consists of ten equally spaced and adjacent steps with depths between 0.1 mm and 1 mm, as seen in figure 1. These steps are 1 cm $\times$ 1 cm in plane, to ensure they are larger than the viewing aperture of our optical measurement equipment. The printing process, shown visually in figure 2, involves filling the plate with a surplus of the pigmented gelatine ink, placing paper onto the filled plate and transferring the ink to the paper by compressing it in a letter press until set. The compression time depends on the amount of gelatine contained in the ink (a larger weight percentage will lead to a shorter setting time) and the bloom of the gelatine (a larger value will set quicker) - here with 17.5 wt% 250 bloom gelatine we only require 5–10 minutes. It is worth noting that all weight percentages are given as a product of the full ink, including water, rather than the weight percentage of the final dried film. As a release agent, lavender oil was applied to the plate prior to printing to ensure that the ink releases from the plate and transfers to the paper surface. We use a glossy photographic micro-porous ink-jet paper (SKU PPD-68) in order to minimize ink absorption by the paper. Each print is repeated three times to ensure we obtain at least one print free from visually-obvious defects, such as bubbles of air that can be trapped in the ink during the printing process or tearing of the print edges, where the printing plate has not been cleanly pulled away.

2.3. CIE $L^*a^*b^*$ measurements

To determine the range of the grayscale, we used a Konica-Minolta FD-7 spectrometer to represent the data in the CIE $L^*a^*b^*$ coordinate system [22]. It is defined by three variables, L^*, a^* and b^*. L^* represents the 'lightness', ranging from 0 (dark) to 100 (light), a^* the green-red and b^* the yellow-blue colour components, that range from -100 to 100, respectively. These are mathematically accessed via the CIE XYZ colour space, comprised of the three tristimulus values X, Y and Z, that are similar but less perceptively uniform.

As we are currently concerned with monochromatic prints, we require only the value of L^*, which is linked to the Y tristimulus value via [23]

$$L^* = 116f\left(\frac{Y}{Y_n}\right) - 16, \tag{1}$$

where $Y_n = 85$, the Y value of the paper substrate we utilise, $\delta = 6/29$ and $f(t) = t^{1/3}$ if $t > \delta^3$ or $f(t) = t/3\delta^3 + 4/29$ if $t < \delta^3$. The tristimulus value Y itself has the form

$$Y = 100\sum_{\lambda} \frac{R(\lambda)I(\lambda)\bar{y}(\lambda)\Delta\lambda}{S(\lambda)\bar{y}(\lambda)\Delta\lambda}, \tag{2}$$

where $I(\lambda)$ is the relative spectral power distribution, $R(\lambda)$ is the spectral reflectance factor and $\bar{y}(\lambda)$ is one of the three colour matching functions used in the CIE XYZ colour space. We utilise a standardized D65 illuminant, intended to represent average daylight with a correlated colour temperature of roughly $T = 6500$ K [22], and so $\bar{y}(\lambda)$ has a form given by the approximation in [24].

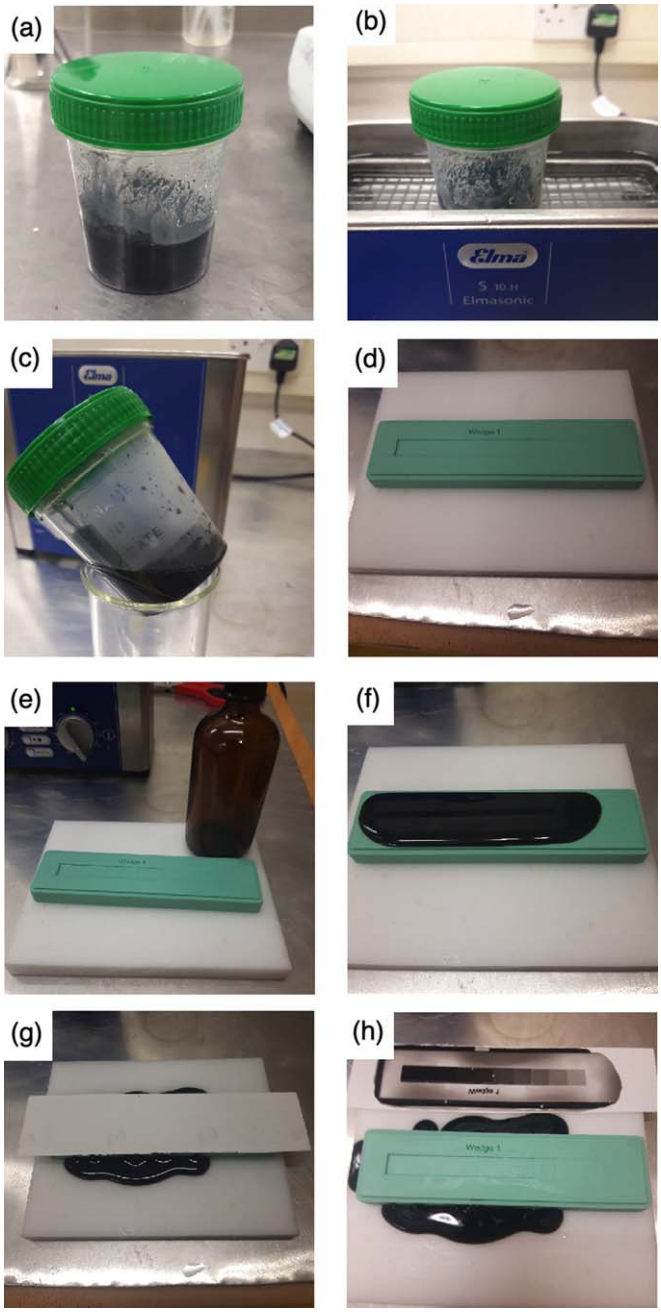

Figure 2. The recreated Woodburytype printing process as we use it. (a) The cooled ink, comprised of gelatine, water and the pigment, is prepared and allowed to set overnight (as described in the ink formulation). (b) A heated ultrasound bath is used to heat the ink to 50 °C and prevent aggregation of the pigment. (c) Once fluid, the ink is ready for use but can be kept in the ultrasound until required. (d) A printing plate, typically a silicon mould, of the required image is used. (e) A release agent (here, lavender oil) is applied to the plate to prevent encourage adhesion to the substrate rather than the plate. (f) The ink is poured onto the plate, ensuring coverage of all troughs in the plate. (g) The paper is placed onto the printing plate and compressed until set. (h) The final print is pulled from the plate and allowed to dry overnight, before any trimming, mounting or cosmetic changes are made.

3. Optical model

3.1. Kubelka-Munk theory

Kubelka-Munk theory is a radiative transfer model that characterises the properties of optically turbid media such as paint or ink films. It models a layer as a homogeneous medium, rather than a ensemble of individual pigment particles, in order to ignore complex multiple-scattering effects and characterises the film with an absorption K and scattering coefficient S, per unit length [25]. It is assumed that these coefficients are uniform throughout the thickness of the film and that there are no prominent edge effects, such that the plane has an effectively infinite width and length.

Multiple attempts have been made to link these Kubelka-Munk (KM) coefficients, K and S, with the properties of the individual pigment particles [23, 26–29], however the exact relationship seems to vary greatly depending on the ratio between K and S. As such, Kubelka-Munk theory is seen as a purely phenomenological approach and is also therefore pigment dependent.

The reflectance $R(\lambda)$ of a film on a substrate can be predicted via these KM coefficients as [27, 30, 31]

$$R = \frac{1 - R_g(a - b\coth bSd)}{a - R_g + b\coth bSd}, \tag{3}$$

where

$$a = \frac{S + K}{S}, \quad b = \sqrt{a^2 - 1}. \tag{4}$$

These equations dictate how the reflectance changes with the substrate reflectance R_g (that ranges between 0 and 1 for a perfectly black and perfectly white diffuser, respectively) and film thickness, d. The general optical properties of carbon black vary minimally within the visible region [32] and so we assume it is effectively constant across these wavelengths.

A common theme of ink film optics is the mis-match between the observed values and predicted values, due to the inherent limitations and assumptions of the Kubelka-Munk theory. One particularly well known facet of this is the loss of light at the interface between the ink film and the air, caused by the change in refractive index of the two materials. The Saunderson correction [33] is employed to correct for this and states that the difference between the measured reflectance (R') and the reflectance predicted by the chosen K and S values (R) is given by [34]

$$R' = \frac{k_1}{2} + (1 - k_1)(1 - k_2)\frac{R}{1 - k_2 R}. \tag{5}$$

Here, k_1 is the fraction of the incident light that is reflected directly from the surface. As such, only $(1 - k_1)$ of the incident light actually enters the print, the rest being immediately reflected. k_2 represents the fraction of light that is incident on the surface from the inside, of which $(1 - k_2)$ emerges from the surface. It is through these re-calculated reflectance values that we can link the CIE $L^*a^*b^*$ values to the KM coefficients and therefore parameterize the inks we are using.

The print height d of the Woodburytype print is of great importance, as it varies to a greater degree than in a traditional print and has a direct control over the amount of absorption and scattering taking place at each point in the print. A known and constant gelatine mass ($m_{gel} = 15$ g) in the ink formulation means that we can produce a simple estimate of the print height, purely from the trough depths of our printing plate. Using the fact that the steps have dimensions $1 \times 1 \times Z$ mm, where Z varies between 0.1 and 1 mm, the ratio between the volume of the gelatine and the total mixture should give us an estimate of the print height once dry. We neglect the presence of carbon as this represents, at most, 1% of the dry mixture. The ratio in this recipe is given by densities of $\rho_{gel} = 1.3$ g cm^{-3} [35] so that the volume of gelatine in the recipe is $V_{gel} = m_{gel}/\rho_{gel} = 11.54$ cm^3 and therefore the ratio is $V_{gel}/V_{tot} = 0.142$. As the steps only vary in depth, we can use this value to link the plate depth to the print height, so that in the deepest step with height 1 mm, the print height should be $d = 0.142 \times 1$ mm $= 0.142$ mm $= 142$ μm. We scale the other steps directly using this same method. Print heights measured by Scanning Electron Microscopy (SEM), shown by the solid line in figure 3, show a similar trend to the above calculation, with a fairly systematic offset. We assume that the difference from the predicted values should be due to water retained during the drying process [36], which is subject to variation under differing drying conditions and gelatine types. The optical path length, that we track the attenuation of the light through, is double this print height.

Figure 4 shows the CIE $L^*a^*b^*$ results for thirteen differing inks, as they vary in print height and carbon black weight percentage. The pigment concentrations increase in rough steps of 0.005% carbon content below 0.02% and in steps of 0.02% above that, to closely map the sharp decay of the data at those lower pigment concentrations and sample less at higher concentrations where the variation between prints is less obvious. The photographic paper used has a CIE $L^*a^*b^*$ brightness of $L^*_{\max} = 93.3$ and provides an upper limit to the data set. As expected, the general trend is an exponential decay toward a minimum value of $L^*_{\min} = 7.1$ with increasing pigment concentration. We use this $L^*_{\min}$ to predict the required value of the Saunderson correction previously mentioned as this represents the case whereby all reflectance occurs due to scattering and reflectance in the immediate vicinity of the surface. In order to attain this value, we use $k_1 = 0.014\,1$ and obtain $k_2 = 0.6$ from [33].

3.2. Single coefficient fitting

Using the equations previously defined for reflectance, we can use the value of the KM coefficients, K and S, in order to predict the L^* curve for a particular concentration. If we assume that all particles dispersed in the

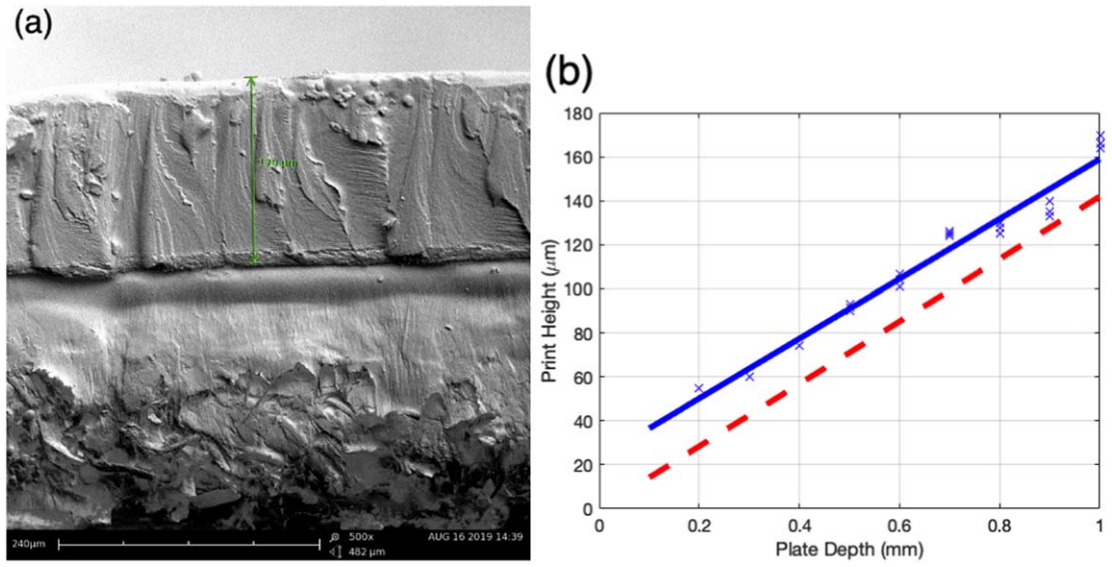

Figure 3. (a) Scanning electron micrograph of the Woodburytype showing an example of the measurement of the gelatine print height, via imaging of the print 'edge-on'. Below the print is the paper, ruptured during the process of drying due to the constriction of the gelatine. (b) Dried print height against the depth of the trough on the printing plate. We take a general trend, the solid line, in order to minimise the local variations in the print height. The dashed line represents the simple estimation method based on the proportion of gelatine in the ink, as described in the text.

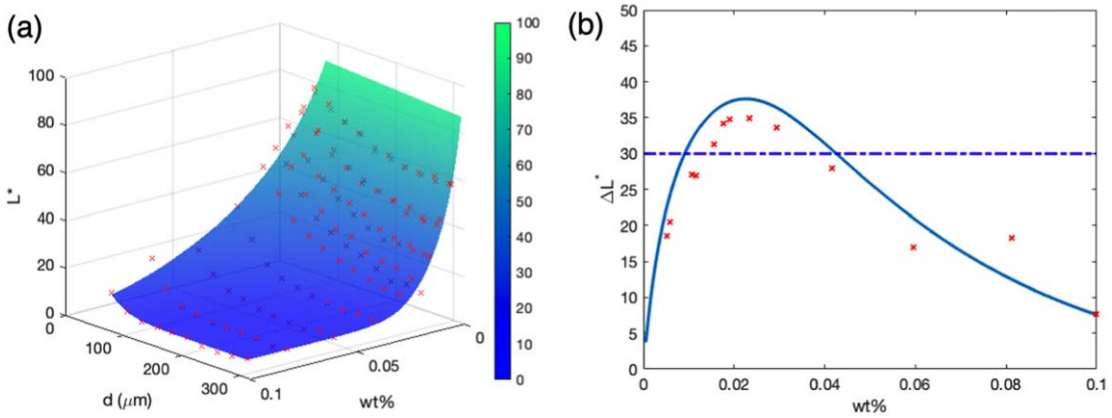

Figure 4. (a) CIE $L^*a^*b^*$ results for step-wedge prints, using inks of varying carbon black weight percentage. The data point points are represented by the red crosses, the single value K/f and S/f fitting is also seen, using values of 5.52 μm^{-1} and 0.01 μm^{-1} respectively. (b) The grayscale ΔL^* of a step-wedge print, calculated as the max difference in L^*, for inks of varying weight percentage and again comparing the data points (red crosses) against the predicted curve (blue line). Also shown, as a dashed line, is the ΔL^* value of an original Woodburytype.

gelatine matrix can be considered identical, we can define the absorption and scattering coefficients within the Kubelka-Munk theory in terms of the absorption and scattering cross sections

$$\frac{K}{f} = \frac{C_{Abs}}{V}, \qquad \frac{S}{f} = \frac{C_{Sca}}{V}, \tag{6}$$

where V is the volume of one such particle and f is the particle volume fraction [32], that can be related to the particle weight fraction F via

$$f = \left[1 + \frac{\rho_{car}}{\rho_{gel}}\left(\frac{1-F}{F}\right)\right]^{-1}, \tag{7}$$

where $\rho_{car} = 1.8\ \mathrm{g\ cm^{-3}}$ (from the manufacturers data sheet, in accordance with Ref. [37]) and $\rho_{gel} = 1.3\ \mathrm{g\ cm^{-3}}$ [35] and a particle weight fraction that varies between 0.03% and 0.6%.

We then use these scaled KM coefficients to predict the L^* curve and use the mean squared error method to characterize the deviation from the data set. With n data points y, alongside the same number of calculated

Table 1. CIE $L^*a^*b^*$ L^* results of 3 Woodburytype inks used; the lowest weight percentage, the largest L^* range and the highest weight percentage.

	Step Depth (mm)									
	0.1	0.2	0.3	0.4	0.5	0.6	0.7	0.8	0.9	1.0
0.005 2 wt%	78.24	73.70	70.34	67.28	63.92	61.40	60.03	59.11	58.86	59.66
0.019 0 wt%	51.96	41.02	33.57	29.37	26.10	24.06	20.76	17.94	18.45	17.25
0.099 9 wt%	16.26	10.59	8.39	8.38	8.49	8.30	7.30	6.59	7.12	8.64

points $\bar{y}$, the mean squared error of such a data set is

$$MSE = \frac{1}{n}\sum_{1}^{n}(y - \bar{y})^2. \tag{8}$$

We minimise this value by varying the variable set $\{K/f, S/f\}$ to provide the best fit for the data set. We find this minima exists for $K/f = 5.52\ \mu\text{m}^{-1}$ and $S/f = 0.01\ \mu\text{m}^{-1}$ and is similar in magnitude to the results found in [32]. The results of this fitting can be seen in figure 4(a), against the original data set.

We can then extend this by plotting the full L^* dependence and discerning the grayscale range of each possible print as the difference between the L^* values of the largest and smallest trough of our step-wedge, such that

$$\Delta L^* = L^*_{\text{max}} - L^*_{\text{min}}, \tag{9}$$

where L^*_{max} lies at the step with maximum depth (1 mm) and L^*_{min} lies at the step with minimum depth (0.1 mm). Figure 4(b) displays the results of such a dependence, comparing both the measured results and the theoretical expectation values, and shows the distinct region of inks that should provide the largest grayscale congregates around a weight percentage of 0.025%. Also shown as a dashed line is the grayscale of an original Woodburytype of Myles Birket Foster ($\Delta L^* = 30$), owned by the Centre for Fine Print Research. The CIE $L^*a^*b^*$ results, averaged across three measurements, for three inks, including one with the largest ΔL^* value, can be seen in table 1.

We can immediately state that our method provides a ΔL^* value larger than that of our estimates of original prints. The original print is free of obvious visual blemishes, however without a destructive method of analysis it is hard to quantify the differences between the print methods, such as the full chemical composition, the print height range or even the substrate used. It is also unknown whether these grayscale values will be affected over large periods of time. We therefore use this comparison merely as a rough benchmark value that we wish to exceed.

3.3. Multiple coefficient fittings

As a first approximation, we have ignored any of optical properties of the binding gelatine that comprises the majority of the print, justified by the hugely absorbent nature of the pigment used. However, it is feasible to assume that as the weight percentage decreases, the optical effects of the gelatine should emerge more prominently and the absorption and scattering coefficients could vary with respect to one another.

We test this assumption by allowing the characteristic absorption and scattering, K/f and S/f, to vary with the weight percentage of the pigment. The results of this process can be seen in figure 5(a) - each print and therefore ink formulation is now described by a unique set of KM coefficients. A comparison to the single coefficient fitting is represented by the dashed lines.

Overall, the values remain somewhat consistent above weight percentages 0.02%, but scattering is greatly enhanced below this value. This could be interpreted as the result of the hand off between the optical properties of the binding gelatine and the highly absorbant pigment. It results in a transition within our model that could explain the underestimation of the average absorption and the near-negligible value of the scattering given by the single coefficient fitting.

In an attempt to construct a finer fit with this data, a more complex fitting can be seen in figure 5(b). Here the absorption is dictated by a linear fitting, in keeping with the standard Kubelka-Munk dependence [32], and the scattering by an exponential, to ensure a smooth decay toward zero at large carbon black weight percentages and an increases at low weight percentages. These again are an approximation of the results obtained based on the look of the data set, but are closer to reality than the single coefficient fitting seen in figure 4(a). The expressions used to define such an empirical fitting are of form

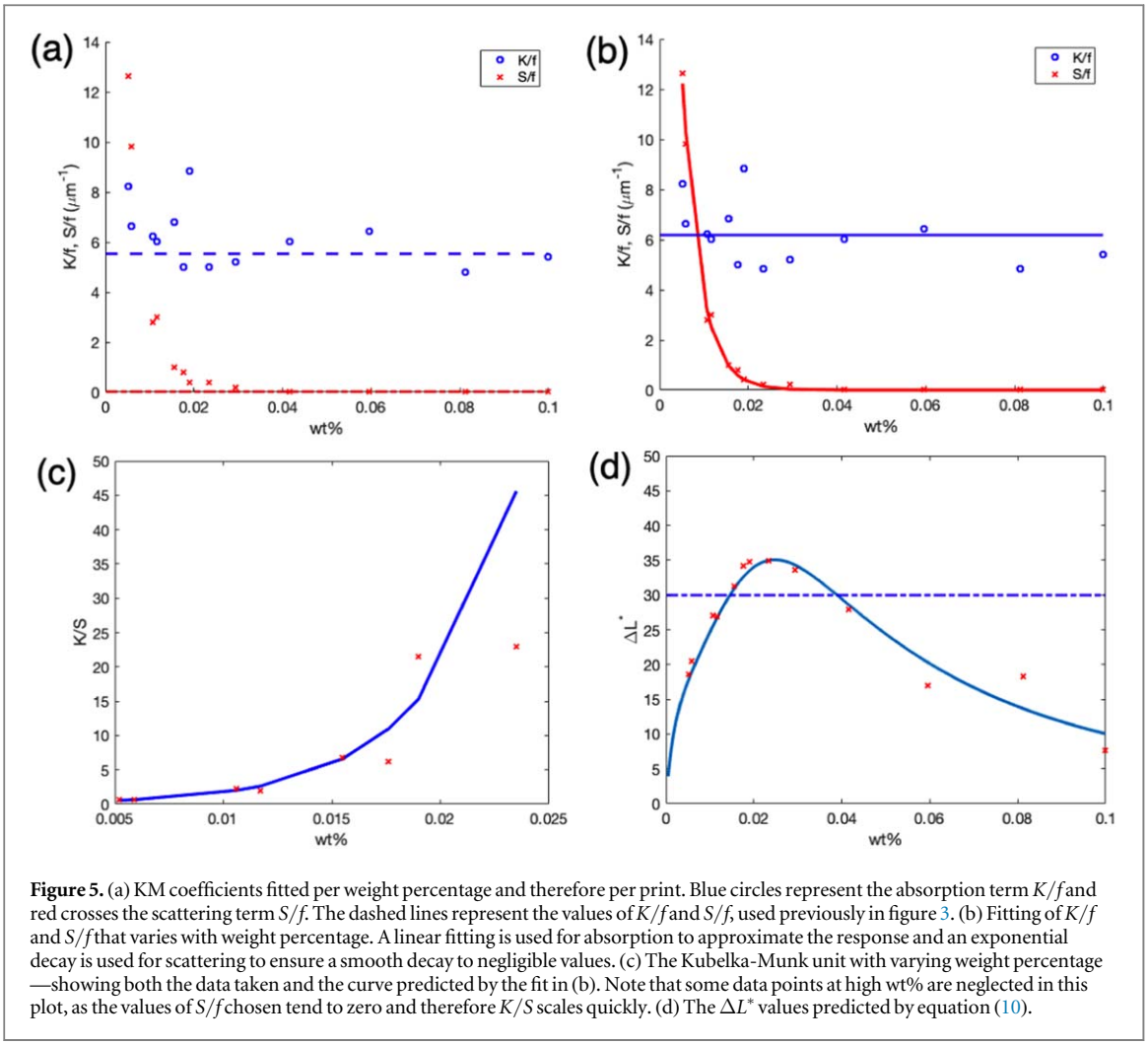

Figure 5. (a) KM coefficients fitted per weight percentage and therefore per print. Blue circles represent the absorption term K/f and red crosses the scattering term S/f. The dashed lines represent the values of K/f and S/f, used previously in figure 3. (b) Fitting of K/f and S/f that varies with weight percentage. A linear fitting is used for absorption to approximate the response and an exponential decay is used for scattering to ensure a smooth decay to negligible values. (c) The Kubelka-Munk unit with varying weight percentage —showing both the data taken and the curve predicted by the fit in (b). Note that some data points at high wt% are neglected in this plot, as the values of S/f chosen tend to zero and therefore K/S scales quickly. (d) The ΔL^* values predicted by equation (10).

$$\frac{K}{f} = (6.19 \times 10^6) \times (wt\%), \quad \frac{S}{f} = (4.36 \times 10^7) \times \exp(-244.49 \times (wt\%)). \tag{10}$$

Notably the Kubelka-Munk unit K/S that results from this, figure 5(c), is non-linear in its dependence on the concentration of the pigment and scales up quickly at high values, in both the data points and the predicted curve. [29] and [32] refer to situations in which the ratio of K/S can increase non-linearly, with the latter pointing to a case involving a highly clustered carbon black pigment and suggesting that this is due to the on-set of multiple scattering events per photon. Conversely, our data suggests that the non-linearity occurs in this system due to the suppression of scattering events from the gelatine binder and hence the increasing dominance of the optical properties of the gelatine with decreasing pigment concentration.

These derived equations can be placed back into equation (3) to obtain reflectance values and then Y and L^* values from equation (2) and equation (1). They allow for a stricter control over the prediction of the ΔL^* values, shown in figure 5(d), and the optical properties of the prints in general.

3.4. Ink prediction

As previously mentioned, the prediction of which ink to use for a given plate is of peak importance in the Woodburytype printing process. As such, using the dependencies in equation (10), we can explore the variation in the grayscale across larger wt% inks and deeper printing plates.

Figure 6 displays how the value of ΔL^* changes and the corresponding wt% ink that produces this, against increasing plate depth (and therefore maximum print height). It shows that we are close to the maximal possible grayscale value in using a 1 mm depth plate (corresponding to 162 μm in print height) and that further increase of the depth of the plate will induce an increase up to $\Delta L^* \approx 40$.

Using a combination of much larger print heights (~300 μm) and lower pigment density, the model suggests it is possible to obtain $\Delta L^* \approx 50$. However, one unintended side-effect of increasing the print height further is that shrinkage of the print in the x- and y-dimension increases [38]. This means that regions of sharp contrast and therefore large vertical variation are smoothed out over greater distances and artefacts of the drying process

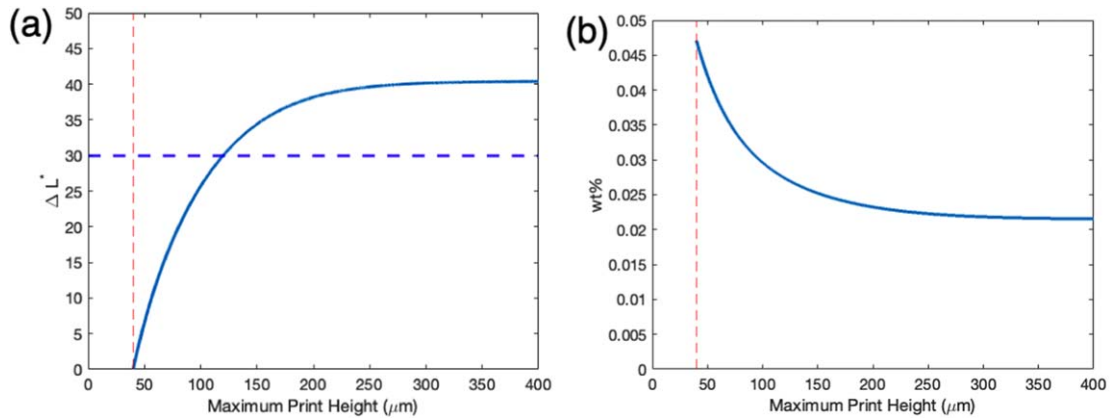

Figure 6. (a) Predicted grayscale range ΔL^* for a range of printing plates, scanning maximum print heights larger than those achievable using the current plate and ink combination. The vertical dashed line represents a minimum print height, discernible over the small variations in print height left behind in the 'white' regions of an image. The horizontal dashed line again indicates the grayscale of an original Woodburytype of Myles Birket Foster. (b) The predicted wt% of carbon black that induces the largest ΔL^* value for a range of print heights. This can then be used to infer the optimal ink formulation per plate.

become more visually obvious, resulting in an inferior replication of the image. Balancing the effects of these drying artefacts with a broad grayscale, alongside the general ease of use provided by the viscosity of the printing ink, means our current formulation is more optimal.

4. Conclusion

To reproduce the high quality of historical Woodburytypes, one important step is to determine the optimal pigment concentration in the ink to generate prints with a good grayscale in the mid-tones. The pigment concentration is correlated to the relief height of the printing plate—the shallower the printing relief, the higher the pigment concentration needed. We used a Kubelka-Munk model for light propagation in the relief of a Woodburytype and found that two methods of fitting CIE L^* data against print height lead to similar values for absorption and scattering coefficients. This allows for a robust characterisation of the carbon black ink we utilise and provides a method of quickly deducing the pigment-load that produces the largest range of L^* values, knowing only the maximal depth of the printing plate. A pigment-load of 0.025 wt% was found to give the maximum difference in the L^* values for a step-wedge printing plate with a relief between 0.1 and 1 mm and this plate depth was found to balance the need for a large grayscale and the minimisation of drying artefacts of the gelatine.

This simple phenomenological model will be used extensively to streamline the ink-making process for future printing plates with different relief depths and can be used as a basis for more complex Woodburytype approaches, such as full colour prints. In this the colour is attained by a traditional multi-colour mixing model such as CMYK (cyan, magenta, yellow and black) but now produced by layering films of coloured semi-transparent gelatine on top of one another. Here, each layer will need to be separately characterised in order to track their individual contributions to not only the lightness L^* but also the colour components a^* and b^*.

Acknowledgments

We acknowledge the support of EPSRC grant EP/R011761/1.

ORCID iDs

D J Leech https://orcid.org/0000-0002-7202-5392

References

[1] Li D, Zhang Y Z and Huang W 2018 Printable transparent conductive films for flexible electronics *Adv. Mat.* **30** 1704738
[2] Li J, Rossignol F and MacDonald J 2015 Inkjet printing for biosensor fabrication: combining chemistry and technology for advanced manufacturing *Lab Chip* **15** 2538–58

[3] Alamán J, Alicante R, Peña J I and Sánchez-Somolinos C 2016 Inkjet printing of functional materials for optical and photonic applications *Materials* **9** 910
[4] Woodbury W B 1864 *Producing Surfaces in Relief, London, Patent 2338*
[5] Crawford W 1979 *The Keepers of Light* (New York: Morgan & Morgan, Dobbs Ferry)
[6] McCallion P 2017 The development of methods for the reproduction in continuous tone of digitally printed colour artworks *PhD Thesis* University of the West of England, Bristol
[7] Leech D J, Guy W and Klein S 2019 The optical properties of the woodburytype—an alternative printing technique based on a gelatine/pigment matrix *Printing for Fabrication* 42-47 (San Francisco)
[8] Pritchard H B 1882 *The Photographic Studios of Europe* (Piper & Carter, London)
[9] Coe B and Haworth-Booth M 1983 *A Guide to Early Photographic Processes* (London: Victoria & Albert Museum)
[10] Ives F E 1884 Photographic block methods *Photographic News* 13
[11] Howe A M 2000 Some aspects of colloids in photography *Current Opinion in Colloid & Interface Science* **5** 288–300
[12] Baziwane D and He Q 2003 Gelatin: the paramount food additive *Food Reviews International* **19** 423–35
[13] Coradin T, Marchal A, Abdoul-Aribi N and Livage J 2005 Gelatine thin films as biomimetic surfaces for silica particles formation *Colloids Surf., B* **44** 191–6
[14] Madaghiele M, Piccinno A, Saponaro M, Maffezzoli A and Sannino A 2009 Collagen-and gelatine-based films sealing vascular prostheses: evaluation of the degree of crosslinking for optimal blood impermeability *J. Mater. Sci., Mater. Med.* **20** 1979–89
[15] Li N, Xue M H, Yao H and Zhu J J 2005 Reagentless biosensor for phenolic compounds based on tyrosinase entrapped within gelatine film *Anal. Bioanal.Chem.* **383** 1127–32
[16] Hoskins S and McCallion P 2014 Continuous tone printing in silicone from CNC milled matrices *Measuring, Modeling, and Reproducing Material Appearance* **9018** 901800
[17] Unknown, The Woodbury Process: Sixth Article, *Photographic News*, II May 1884
[18] Dusan A K and Stulik C 2013 *Woodburytype* (Los Angeles: The Getty Conservation Institute)
[19] Calixto S, Ganzherli N, Gulyaev S and Figueroa-Gerstenmaier S 2018 Gelatin as a photosensitive material *Molecules* **23** 2064
[20] Basha M A F 2019 Optical properties and colorimetry of gelatine gels prepared in different saline solutions *J. Adv. Res.* **16** 55–65
[21] Pang Z, Deeth H, Sopade P, Sharma R and Bansala N 2014 Rheology, texture and microstructure of gelatin gels with and without milk proteins *Food Hydrocolloids* **35** 484–93
[22] Schanda J 2006 *Colorimetry: Understanding the CIE System* (Vienna: CIE Central Bureau)
[23] McNeil L E and French R H 2000 Light scattering from red pigment particles: multiple scattering in a strongly absorbing system *J. Appl. Phys.* **89** 1
[24] Wyman C, Sloan P P and Shirley P 2013 Simple analytic approximations to the CIE XYZ color matching functions *Journal of Computer Graphics Techniques* **2** 2
[25] Kubelka P and Munk F 1931 Ein beitrag zur optik der farbanstriche *Zeitschrift für Technische Physik* **12** 593–601
[26] Mudgett P S and Richards L W 1971 Multiple scattering calculations for technology *Appl. Opt.* **10** 1485–502
[27] Quinten M 2001 The color of finely dispersed nanoparticles *Appl. Phys.* B **73** 317–26
[28] Yang L and Kruse B 2004 Revised Kubelka-Munk theory. I. theory and application *J. Opt. Soc. Am.* A **21** 1933–41
[29] Granberg H and Edström P 2003 Quantification of the intrinsic error of the Kubelka-Munk model caused by strong light absorption *J. Pulp Pap. Sci.* **29** 386–90
[30] Gunde M K, Logar J K, Orel Z C and Orel B 1995 Application of the Kubelka-Munk theory to thickness-dependent diffuse reflectance of black paints in the mid-IR *Appl. Spectrosc.* **43** 623–9
[31] Koirala P, Hauta-Kasari M, Martinkauppi B and Hiltunen J 2008 Color mixing and color separation of pigments with concentration prediction *Color Research and Application* **33** 461–9
[32] Tesfamichael T, Hoel A, Niklasson G A, WäckelgÅrd E, Gunde M K and Orel Z C 2001 Optical characterization method for black pigments applied to solar-selective absorbing paints *Appl. Opt.* **40** 1672–81
[33] Saunderson J L 1942 Calculation of the color of pigmented plastics *Jour. of Opt. Soc. Am.* **32** 727
[34] Orel Z C, Gunde M K and Ore1 B 1997 Application of the Kubelka-Munk theory for the determination of the optical properties of solar absorbing paints *Prog. Org. Coat.* **30** 49–66
[35] Parker N G and Povey M J W 2012 Ultrasonic study of the gelation of gelatin: phase diagram, hysteresis and kinetics *Food Hydrocolloids* **26** 99–107
[36] Chiou B-S, Avena-Bustillos R J, Bechtel P J, Imam S H, Glenn G M and Ortsa W J 2009 Effects of drying temperature on barrier and mechanical properties of cold-water fish gelatin films *J. Food Eng.* **95** 327–31
[37] Lu, S. and Chung, D.D.L., 2013. Viscoelastic behavior of carbon black and its relationship with the aggregate size. Carbon, 60, pp.346-355.
[38] Navarrete-García E and Calixto S 2003 Continuous surface relief micro-optical elements fabricated on photographic emulsions by use of binary and halftone masks *Opt. Mater.* **23** 501–12